Dark matter in minimal supergravity with type-II seesaw mechanism

J. N. Esteves,[*] S. Kaneko,[†] and J. C. Romao[‡]

Departamento de Física and CFTP, Instituto Superior Técnico, Avenida Rovisco Pais 1, 1049-001 Lisboa, Portugal

M. Hirsch[§]

AHEP Group, Instituto de Física Corpuscular—CSIC/Universitat de València, Edificio de Institutos de Paterna, Apartado 22085, E-46071 València, Spain

W. Porod[‖]

Institut für Theoretische Physik und Astronomie, Universität Würzburg, Am Hubland, 97074 Wuerzburg

We calculate the relic density of the lightest neutralino in a supersymmetric seesaw type-II ("triplet seesaw") model with minimal supergravity boundary conditions at the grand unified theory (GUT) scale. The presence of a triplet below the GUT scale, required to explain measured neutrino data in this setup, leads to a characteristic deformation of the sparticle spectrum with respect to the pure minimal supergravity (mSUGRA) expectations, affecting the calculated relic dark matter (DM) density. We discuss how the DM allowed regions in the $(m_0, M_{1/2})$ plane change as a function of the (type-II) seesaw scale. We also compare the constraints imposed on the models parameter space form upper limits on lepton flavor violating decays to those imposed by DM. Finally, we briefly comment on uncertainties in the calculation of the relic neutralino density due to uncertainties in the measured top and bottom masses.

I. INTRODUCTION

Standard cosmology requires the existence of a non-baryonic dark matter (DM) contribution to the total energy budget of the universe [1,2]. In the past few years estimates of the DM abundance have become increasingly precise. Indeed, the Particle Data Group now quotes at 1σ C.L. [3]

$$\Omega_{\mathrm{DM}} h^2 = 0.105 \pm 0.008. \tag{1}$$

Since the data from the WMAP satellite [4,5] and large scale structure formation [6] are best fitted if the DM is cold, weakly interacting mass particles (WIMP) are currently the preferred explanation. While there is certainly no shortage of WIMP candidates (lists can be found in many reviews, see for example [1,2,7,8]), the literature is completely dominated by studies of the lightest neutralino.

Neutrino oscillation experiments have shown that neutrinos have nonzero mass and mixing angles [9–13] and the most recent global fits to all data [14] confirm again that the mixing angles are surprisingly close to the so-called tribi-maximal mixing (TBM) values [15]. In the minimal supersymmetric extension of the standard model (MSSM) with conserved R-parity neutrino masses are zero for the same reasons as in the SM. However, it was shown long ago that

if neutrinos are Majorana particles, their mass is described by a unique dimension-5 operator [16]

$$m_\nu = \frac{f}{\Lambda}(HL)(HL). \tag{2}$$

All (Majorana) neutrino mass models reduce to this operator at low energies. If f is a coefficient $\mathcal{O}(1)$, current neutrino data indicate $\Lambda \lesssim \mathcal{O}(10^{15})$ GeV. This is the essence of the "seesaw" mechanism. There are three different tree-level realizations of the seesaw, classified as type-I, type-II and type-III in [17]. Type-I is the well-known case of the exchange of a heavy fermionic singlet [18–20]. Type-II corresponds to the exchange of a scalar triplet [21–24]. One could also add one (or more) fermionic triplets to the field content of the SM [25]. This is called seesaw type-III in [17].

Neutrino experiments at low energies measure only $f_{\alpha\beta}/\Lambda$, thus observables outside the neutrino sector will ultimately be needed to learn about the origin of Eq. (2). Augmenting the SM with a high-scale seesaw mechanism does not lead to any conceivable phenomenology apart from neutrino masses, but if weak scale supersymmetry exists *indirect* probes into the high energy world might be possible. Two kinds of measurements containing such indirect information exist in principle, lepton flavor violating (LFV) observables and sparticle masses.

Assuming complete flavor blindness in the soft supersymmetry breaking parameters at some large scale, the neutrino Yukawa matrices will, in general, lead to nonzero

[*]joaomest@cftp.ist.utl.pt
[†]satoru@cftp.ist.utl.pt
[‡]jorge.romao@ist.utl.pt
[§]mahirsch@ific.uv.es
[‖]porod@physik.uni-wuerzburg.de

flavor violating entries in the slepton mass matrices, if the seesaw scale is lower than the scale at which supersymmetry (SUSY) is broken. This was first pointed out in [26]. The resulting LFV processes have been studied in many publications, for low-energy observables such as $\mu \to e\gamma$ and $\mu - e$ conversion in seesaw type-I, see for example [27–33], for seesaw type-II [34,35]. LFV collider observables have also been studied in a number of papers, see for example [35–47].

Mass measurements in the sparticle sector will not only be necessary to learn about the mechanism of SUSY breaking in general, but might also reveal indications about the scale of the seesaw mechanism. However, very precise knowledge of masses will be necessary before one can learn about the high-scale parameters [48,49]. Especially interesting in this context is the observation that from the different soft scalar and gaugino masses one can define certain combinations (''invariants'') which are nearly constant over large parts of minimal supergravity (mSUGRA) space. Adding a seesaw mechanism of type-II or type-III these invariants change in a characteristic way as a function of the seesaw scale and are thus especially suited to extract information about the high energy parameters [50]. Note, however, that the invariants are constants in mSUGRA space only in leading order and that quantitatively important 2-loop corrections exist [35].

In this paper we study neutralino dark matter [51–53] within a supersymmetric type-II seesaw model with mSUGRA boundary conditions. For definiteness, the model we consider consists of the MSSM particle spectrum to which we add a single pair of **15**- and $\overline{\textbf{15}}$-plets. This is the simplest supersymmetric type-II setup, which allows one to maintain gauge coupling unification [34] and explain measured neutrino oscillation data.

In mSUGRA—assuming a standard thermal history of the early universe[1]—only four very specific regions in parameter space can correctly explain the most recent WMAP data [5]. These are (i) the bulk region; (ii) the coannihilation line; (iii) the ''focus point'' line; and (iv) the ''Higgs funnel'' region. In the bulk region there are no specific relations among the sparticle masses. However, all sparticles are rather light in this region, so it is already very constrained from the viewpoint of low-energy data [55]. In the coannihilation line the lightest scalar tau is nearly degenerate with the lightest neutralino, thus reducing the neutralino relic density with respect to naive expectations [52,56]. In the ''focus point'' line [56,57] $\Omega_{\chi_1^0} h^2$ is small enough to explain $\Omega_{\text{DM}} h^2$ due to a rather small value of μ leading to an enhanced Higgsino component in the lightest neutralino and thus an enhanced coupling to the Z^0 boson. Lastly, at large $\tan\beta$ an s-channel resonance pair annihila-

tion of neutralinos through the *CP*-odd Higgs boson can become important. This is called the Higgs funnel region [53].

The addition of the **15** and $\overline{\textbf{15}}$ pair at the high scale does not, in general, lead to the appearance of new allowed regions. However, the deformed sparticle spectrum with respect to mSUGRA expectations leads to characteristic changes in the allowed regions as a function of the unknown seesaw scale. We discuss these changes in detail and compare the results to other indirect constraints, namely, the observed neutrino masses and upper limits on LFV processes. We concentrate on the seesaw type-II scheme, since for mSUGRA + seesaw type-I the changes in the DM allowed regions with respect to pure mSUGRA are, in general, expected to be tiny.[2]

The rest of this paper is organized as follows. In the next section we briefly summarize the main ingredients of the model and give a short discussion of mSUGRA and the expected changes in sparticle masses in our setup with respect to mSUGRA. In Sec. III we present our numerical results. This is the main section of this paper, where we discuss in detail how the introduction of a **15** changes the predicted DM abundance as a function of the seesaw scale. We also confront the DM allowed regions with constraints from nonobservation of LFV processes and briefly comment on DM in mSUGRA with a seesaw type-I. We then close with a short summarizing discussion in Sec. IV.

II. SETUP: MSUGRA AND $SU(5)$ MOTIVATED TYPE-II SEESAW

In this section we summarize the main features of the model we will use in the numerical calculation. We will always refer to mSUGRA as the ''standard'' against which we compare all our results. More precisely, by mSUGRA we mean the MSSM with universal boundary conditions at the grand unified theory (GUT) scale, sometimes referred to as the constrained minimal supersymmetric standard model (CMSSM). The model consists in extending the MSSM particle spectrum by a pair of **15** and $\overline{\textbf{15}}$.[3] It is the minimal supersymmetric seesaw type-II model which maintains gauge coupling unification [34].

mSUGRA is specified by 4 continuous and one discrete parameter [60]. These are usually chosen to be m_0, the common scalar mass, $M_{1/2}$, the gaugino mass parameter, A_0, the common trilinear parameter, $\tan\beta = \frac{v_2}{v_1}$ and the sign of μ. m_0, $M_{1/2}$ and A_0 are defined at the GUT scale, the

---

[1]In models with nonstandard thermal history the relation between sparticle masses and relic density can be lost completely [54].

[2]We have confirmed this general expectation with some sample calculations. However, an exceptional case has been presented recently in [58], see the more detailed discussion in Sec. III.

[3]In this model the **15** and $\overline{\textbf{15}}$ are potential candidates for supersymmetry mediation and in order not to dominate over gravity we assume that they are weakly coupled to the hidden sector [59].

renormalization group equations (RGEs) are known at the 2-loop level [61].

Under $SU(3) \times SU_L(2) \times U(1)_Y$ the **15** decomposes as

$$\mathbf{15} = S + T + Z$$

$$S \sim \left(6, 1, -\frac{2}{3}\right), \qquad T \sim (1, 3, 1), \qquad Z \sim \left(3, 2, \frac{1}{6}\right). \tag{3}$$

The $SU(5)$ invariant superpotential reads as

$$W = \frac{1}{\sqrt{2}} \mathbf{Y}_{15} \bar{5} \cdot 15 \cdot \bar{5} + \frac{1}{\sqrt{2}} \lambda_1 \bar{5}_H \cdot 15 \cdot \bar{5}_H$$
$$+ \frac{1}{\sqrt{2}} \lambda_2 5_H \cdot \overline{15} \cdot 5_H + \mathbf{Y}_5 10 \cdot \bar{5} \cdot \bar{5}_H$$
$$+ \mathbf{Y}_{10} 10 \cdot 10 \cdot 5_H + M_{15} 15 \cdot \overline{15} + M_5 \bar{5}_H \cdot 5_H. \tag{4}$$

Here, $\bar{5} = (d^c, L)$, $10 = (u^c, e^c, Q)$, $5_H = (t, H_2)$ and $\bar{5}_H = (\bar{t}, H_1)$. Below the GUT scale in the $SU(5)$-broken phase the potential contains the terms

$$\frac{1}{\sqrt{2}} (Y_T L T_1 L + Y_S d^c S d^c) + Y_Z d^c Z L + Y_d d^c Q H_1$$
$$+ Y_u u^c Q H_2 + Y_e e^c L H_1$$
$$+ \frac{1}{\sqrt{2}} (\lambda_1 H_1 T_1 H_1 + \lambda_2 H_2 T_2 H_2) + M_T T_1 T_2 + M_Z Z_1 Z_2$$
$$+ M_S S_1 S_2 + \mu H_1 H_2 \tag{5}$$

Y_d, Y_u and Y_e generate quark and charged lepton masses in the usual manner. In addition there are the matrices Y_T, Y_S and Y_Z. For the case of a complete **15**, apart from calculable threshold corrections, $Y_T = Y_S = Y_Z$ and M_T, M_S and M_Z are determined from M_{15} by the RGEs. As long as $M_Z \sim M_S \sim M_T \sim M_{15}$ gauge coupling unification will be maintained. The equality need not be exact for successful unification.

The triplet T_1 has the correct quantum numbers to generate neutrino masses via the first term in Eq. (5). Integrating out the heavy triplets at their mass scale a dimension-5 operator of the form Eq. (2) is generated and after electroweak symmetry breaking (EWSB) the resulting neutrino mass matrix can be written as

$$m_\nu = \frac{v_2^2}{2} \frac{\lambda_2}{M_T} Y_T. \tag{6}$$

Here v_2 is the vacuum expectation value of Higgs doublet H_2 and we use the convention $\langle H_i \rangle = \frac{v_i}{\sqrt{2}}$. m_ν can be diagonalized in the standard way with a unitary matrix U, containing in general 3 angles and 3 phases. Note that $\hat{Y}_T = U^T \cdot Y_T \cdot U$ is diagonalized by *the same matrix as* m_ν. This means that if all neutrino eigenvalues, angles and phases were known, Y_T would be completely fixed up to an overall constant, which can be written as $\frac{M_T}{\lambda_2} \simeq 10^{15}$ GeV $\left(\frac{0.05 \text{ eV}}{m_\nu}\right)$. Thus, current neutrino data require M_T

to be lower than the GUT scale by (at least) an order or magnitude.

The full set of RGEs for the **15** + $\overline{\mathbf{15}}$ can be found in [34] and in the numerical calculation, presented in the next section, we solve the exact RGEs. However, for a qualitative understanding of the results, the following approximative solutions are quite helpful.

For the gaugino masses one finds in leading order

$$M_i(m_{\text{SUSY}}) = \frac{\alpha_i(m_{\text{SUSY}})}{\alpha(M_G)} M_{1/2}. \tag{7}$$

Equation (7) implies that the ratio M_2/M_1, which is measured at low energies, has the usual mSUGRA value, but the relationship to $M_{1/2}$ is changed. Neglecting the Yukawa couplings $\mathbf{Y}_{15}$ (see below), for the soft mass parameters of the first two generations one gets

$$m_{\tilde{f}}^2 = M_0^2 + \sum_{i=1}^{3} c_i^{\tilde{f}} \left(\left(\frac{\alpha_i(M_T)}{\alpha(M_G)} \right)^2 f_i + f_i' \right) M_{1/2}^2, \tag{8}$$

$$f_i = \frac{1}{b_i} \left(1 - \left[1 + \frac{\alpha_i(M_T)}{4\pi} b_i \log \frac{M_T^2}{m_Z^2} \right]^{-2} \right),$$

$$f_i' = \frac{1}{b_i + \Delta b_i} \left(1 - \left[1 + \frac{\alpha(M_G)}{4\pi} (b_i + \Delta b_i) \log \frac{M_G^2}{M_T^2} \right]^{-2} \right). \tag{9}$$

The various coefficients $c_i^{\tilde{f}}$ can be found in [35]. The gauge couplings are given as

$$\alpha_1(m_Z) = \frac{5\alpha_{\text{em}}(m_Z)}{3\cos^2\theta_W},$$

$$\alpha_2(m_Z) = \frac{\alpha_{\text{em}}(m_Z)}{\sin^2\theta_W},$$

$$\alpha_i(m_{\text{SUSY}}) = \frac{\alpha_i(m_Z)}{1 - \frac{\alpha_i(m_Z)}{4\pi} b_i^{SM} \log \frac{m_{\text{SUSY}}^2}{m_Z^2}},$$

$$\alpha_i(M_T) = \frac{\alpha_i(m_{\text{SUSY}})}{1 - \frac{\alpha_i(m_{\text{SUSY}})}{4\pi} b_i \log \frac{M_T^2}{m_{\text{SUSY}}^2}}, \tag{10}$$

$$\alpha_i(M_G) = \frac{\alpha_i(M_T)}{1 - \frac{\alpha_i(M_T)}{4\pi} (b_i + \Delta b_i) \log \frac{M_G^2}{M_T^2}},$$

with b_i^{SM} and b_i^{MSSM} being the usual standard model and MSSM coefficients. $\Delta b_i = 7$ for all i in the case of a complete 15-plet.

We can estimate the soft mass parameters given the above formulas for a given choice of m_0, $M_{1/2}$ and $M_{15} = M_T$. We show some arbitrarily chosen examples in Fig. 1. Note that the result shown is approximate, since we are (a) using the leading log approximation and (b) two loop effects are numerically important, especially for m_Q, but not included. The figure serves to show that for any $M_{15} < M_{\text{GUT}}$ the resulting mass parameters are always smaller
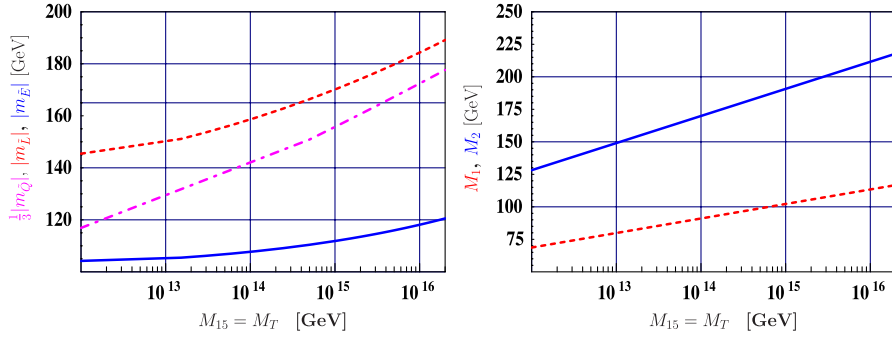
FIG. 1 (color online).   Analytically calculated running of scalar (to the left) and gaugino mass parameters (to the right), leading order only. The mass parameters are calculated as a function of M_{15} for the mSUGRA parameters $m_0 = 70$ GeV and $M_{1/2} = 250$ GeV. For $M_{15} \simeq 2 \times 10^{16}$ GeV the mSUGRA values are recovered. Smaller M_{15} lead to smaller soft masses in all cases. Note that the running is different for the different mass parameters with gaugino masses running faster than slepton mass parameters.

than the mSUGRA expectations for the same choice of initial parameters $(m_0, M_{1/2})$. While the exact values depend on $(m_0, M_{1/2})$ and on the other mSUGRA parameters, this feature is quite generally true in all of the $(m_0, M_{1/2})$ plane. Note that the running is different for the different scalar mass parameters, but the ratio of the gaugino mass parameters M_1/M_2 always stays close to the mSUGRA expectation, $M_1 \simeq \frac{5}{3} \tan^2\theta_W M_2$.

III. NUMERICAL RESULTS

In this section we discuss our numerical results. All the plots shown below are based on the program packages SPHENO [62] and MICROMEGAS [63,64]. We use SPHENO V3 [65], including the RGEs for the **15** + $\overline{\mathbf{15}}$ case [34,35] at the 2-loop level for gauge couplings and gaugino masses and at one-loop level for the remaining MSSM parameters and the 15-plet parameters, for a discussion see [35]. For any given set of mSUGRA and 15-plet parameters SPHENO calculates the supersymmetric particle spectrum at the electroweak scale, which is then interfaced with MICROMEGAS 2.2 [66] to calculate the relic density of the lightest neutralino, $\Omega_{\chi_1^0}h^2$.

For the standard model parameters we use the Particle Data Group 2008 values [3], unless specified otherwise. As discussed below, especially important are the values (and errors) of the bottom and top quark masses, $m_b = 4.2 + 0.17 - 0.07$ GeV and $m_t = 171.2 \pm 2.1$ GeV. Note that the m_t is understood to be the pole mass and $m_b(m_b)$ is the $\overline{\text{MS}}$ mass. As the allowed range for $\Omega_{\text{DM}}h^2$ we always use the 3σ C.L. boundaries as given in [3], i.e. $\Omega_{\text{DM}}h^2 = [0.081, 0.129]$. Note, however, that the use of 1σ contours results in very similar plots, due to the small error bars.

In the "seesaw sector" we have the parameters connected with the 15-plets, i.e. M_{15}, Y_{15}, λ_1 and λ_2. For the calculation of the dark matter abundance the most important parameter is M_{15}. It has turned out that the effects of Y_{15}, λ_1 and λ_2 on the relic abundance of neutralinos are

very minor. Note, however, that as discussed in the previous section, atmospheric neutrino oscillation data cannot be explained in our setup, if the triplet mass is larger than approximately $M_{15} = M_T = 10^{15}$ GeV. Also, the nonobservation of LFV decays puts an upper bound on M_{15}. The latter, however, is strongly dependent on $\tan\beta$ and depends also on m_0 and $M_{1/2}$. We will first show results using different values of M_T as free parameter, without paying attention to neutrino masses and LFV. We will discuss how our results change for correctly fitted neutrino masses and angles towards the end of this section, where we also discuss and compare LFV excluded regions with DM allowed ones.

We define our "standard choice" of mSUGRA parameters as $\tan\beta = 10$, $A_0 = 0$ and $\mu > 0$ and use these values in all plots, unless specified otherwise. We then show our results in the plane of the remaining two free parameters, $(m_0, M_{1/2})$. Figure 2 shows in the top panel contours of equal dark matter density, $\Omega_{\chi_1^0}h^2$. The lines are constant $\Omega_{\chi_1^0}h^2$ with $\Omega_{\chi_1^0}h^2 = 0.1, 0.2, 0.5, 1, 2$. In the bottom panel we show the range of parameters allowed by the DM constraint at 3σ C.L. In both cases, to the left a pure mSUGRA calculation, whereas the plot to the right shows mSUGRA + 15-plet with $M_T = 10^{14}$ GeV. In each plot the yellow (shaded) regions are eluded either by the lighter scalar tau being the lightest supersymmetric particle (LSP) (to the bottom right) or by the LEP limit on the mass of the lighter chargino (to the left), $m_{\chi_1^+} \geq 105$ GeV. In addition, we show two lines of constant lightest Higgs boson mass, $m_{h^0} = 110$ GeV (dotted lines) and $m_{h^0} = 114.4$ GeV (dashed lines), as calculated by SPHENO, see the discussion below.

The plots show three of the different allowed regions discussed in the Introduction. To the right the coannihilation region, here the lightest neutralino and the lighter scalar tau are nearly degenerate in mass. The line going nearly vertically upwards at constant $M_{1/2}$ is the "focus point" line. The small region connecting the two lines is
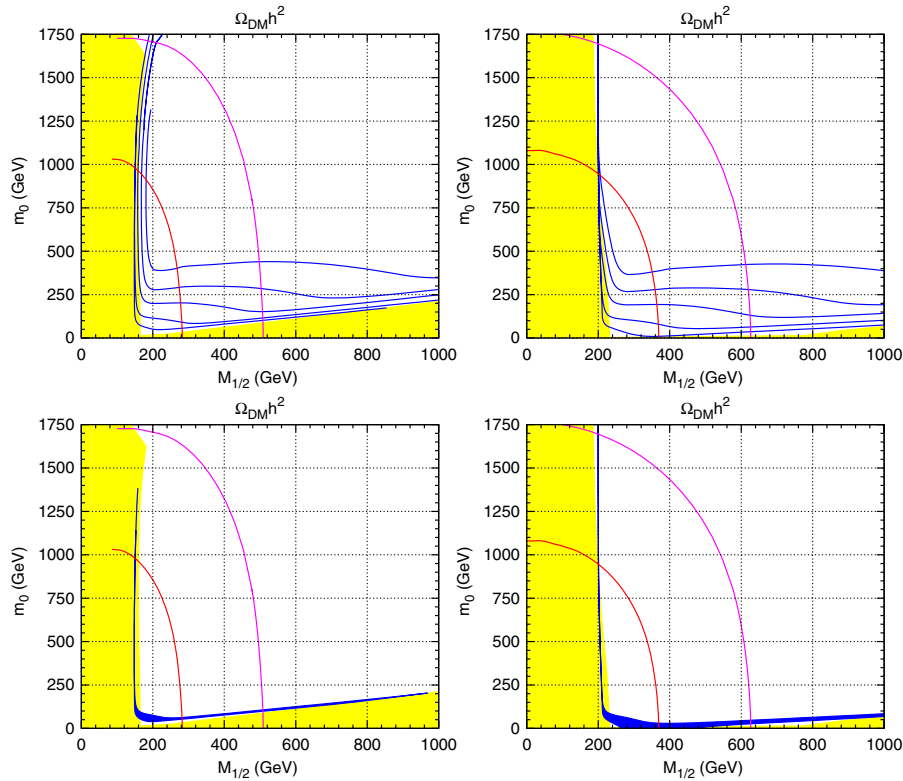
FIG. 2 (color online).   Top: Contours of equal dark matter density ($\Omega_{\chi_1^0}h^2$) in the (m_0, $M_{1/2}$) plane for the "standard choice" $\tan\beta = 10$, $A_0 = 0$ and $\mu \geq 0$, for mSUGRA (left panel) and type-II seesaw with $M_T = 10^{14}$ GeV (right panel). The lines are constant $\Omega_{\chi_1^0}h^2$ with $\Omega_{\chi_1^0}h^2 = 0.1, 0.2, 0.5, 1, 2$. Bottom: Range of parameters allowed by the DM constraint at 3σ C.L. To the left: mSUGRA; to the right: $M_T = 10^{14}$ GeV. For a discussion see text.

the remains of the bulk region, which has shrunk considerably due to the reduced error bars on $\Omega_{DM}h^2$ after the most recent WMAP data [5]. The focus point line is excluded by the LEP constraint on the lighter chargino mass at low and moderate values of m_0. It becomes allowed only at values of m_0 larger than (very roughly) 1–1.5 TeV. However, note that the exact value of m_0 at which the focus point line becomes allowed is extremely sensitive to errors in $m_{\chi_1^+}$, both from the experimental bound and the error in the theoretical calculation.

Comparing the results for the pure mSUGRA case to the mSUGRA + 15-plet calculation, two differences are immediately visible in Fig. 2. First, the focus point line is shifted towards larger values of $M_{1/2}$. This is due to the fact that for the 15-plet at $M_{15} = 10^{14}$ GeV the neutralino is lighter than in the mSUGRA case at the same value of $M_{1/2}$, compare to Fig. 1. Maintaining the same relation between M_1 and μ as in the mSUGRA case requires then a larger value of $M_{1/2}$. Note that for the same reason the excluded region from the LEP bound on the chargino mass is larger than in the mSUGRA case. Second, on finds that the coannihilation line is shifted towards smaller values of m_0. The latter can be understood from Fig. 3.

Figure 3 shows the allowed region for the dark matter density in the (m_0, $M_{1/2}$) plane for our "standard choice"

of other mSUGRA parameters for a number of different M_T (to the left). The plot shows how the coannihilation line moves towards smaller values of m_0 for smaller values of M_T. The plot on the right in Fig. 3 explains this behavior. It shows the variation of the mass difference $m_{\tilde{\tau}_1} - m_{\chi_0}$ (top lines) and of Ωh^2 (bottom lines), as a function of M_T for four different values of m_0: 0 (cyan), 50 (magenta), 100 (blue) and 150 GeV (green) for one fixed value of $M_{1/2} = 800$ GeV. The yellow region corresponds to the experimentally allowed DM region. Coannihilation requires a small value of $m_{\tilde{\tau}_1} - m_{\chi_0}$, typically smaller than a few GeV. With decreasing values of M_T the gaugino masses run down to smaller values faster than the slepton masses, thus effectively increasing $m_{\tilde{\tau}_1} - m_{\chi_0}$ in these examples with respect to mSUGRA. To compensate for this effect at constant $M_{1/2}$ smaller values of m_0 are required to get the $m_{\tilde{\tau}_1} - m_{\chi_0}$ in the required range.

At this point a short discussion of the Higgs boson mass bound might be in order. LEP excluded a light Higgs boson with SM couplings with masses below $m_h \lesssim 114.4$ GeV [3]. For reduced coupling of the Higgs boson to $b\bar{b}$ the bound is less severe, so this bound is not strictly valid in all of MSSM space. More important for us, however, is the *theoretical* uncertainty in the calculation of the lightest Higgs boson mass. SPHENO calculates m_{h^0} at two-loop level
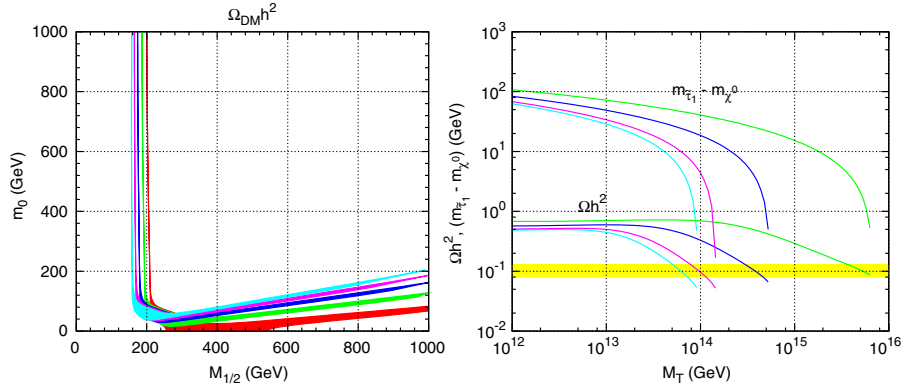
FIG. 3 (color online). Allowed region for dark matter density ($0.081 < \Omega_{\chi_1^0} h^2 < 0.129$) in the ($m_0, M_{1/2}$) plane for the "standard choice" $\tan\beta = 10$, $A_0 = 0$ and $\mu \geq 0$, for five values from M_T, $M_T = 10^{14}$ GeV (red), to $M_T = 10^{16}$ GeV (cyan), to the left. To the right: Variation of the mass difference $m_{\tilde{\tau}_1} - m_{\chi_0}$ (top lines) and of Ωh^2 (bottom lines), as a function of M_T for four different values of m_0: 0 (cyan), 50 (magenta), 100 (blue) and 150 GeV (green) for one fixed value of $M_{1/2} = 800$ GeV. The yellow region corresponds to the experimentally allowed DM region.

using $\overline{\text{DR}}$ renormalization. Expected errors for this kind of calculation, including a comparison of different public codes, have been discussed in [67]. As discussed in [67,68] even at the 2-loop level uncertainties in the calculation of m_{h^0} can be of the order of 3–5 GeV. In this context it is interesting to note that FEYNHIGGS [69], which calculates the Higgs masses in a diagrammatic approach within the $\overline{\text{OS}}$ renormalization scheme tends to predict Higgs masses which are systematically larger by 3–4 GeV, when compared with the $\overline{\text{DR}}$ calculation. We therefore showed in Fig. 2 two lines of constant Higgs boson masses. The value of $m_{h^0} = 114.4$ GeV is taking the LEP bound at face value, while the lower value of $m_{h^0} = 110$ GeV estimates the parameter region which is excluded *conservatively*, including the theoretical error. Since the lightest Higgs boson mass varies slowly with m_0 and $M_{1/2}$, even a relatively tiny change in m_{h^0} of, say 1 GeV, shifts the extreme values of the excluded region by ~ 50 GeV in $M_{1/2}$ (at small m_0) and by ~ 150 GeV in m_0 (at small $M_{1/2}$).

Moreover, it is well known that the calculated Higgs boson masses are strongly dependent on the mixing in the stop sector and thus, indirectly, on the value of A_0. This is shown for the case of a pure mSUGRA calculation in Fig. 4. Here we show two examples for the DM allowed region and the regions disfavored by the Higgs boson mass bound at $m_{h^0} = 114.4$ GeV and $m_{h^0} = 110$ GeV. Larger negative A_0 leads to a less stringent constraint (for $\mu > 0$). Note that all of the bulk region becomes allowed at $A_0 = -500$ GeV, once the theoretical uncertainty in the Higgs boson mass calculation is taken into account. We have checked for a few values of M_T that for the case of mSUGRA + **15** the resulting Higgs boson bounds are very similar. We thus do not repeat the corresponding plots here. Comparing the calculations shown in Fig. 4 and the mSUGRA calculation in Fig. 2 with each other, one finds that the DM allowed regions are actually affected very little by the choice of A_0. We have checked that this is also the case for mSUGRA + seesaw type-II.

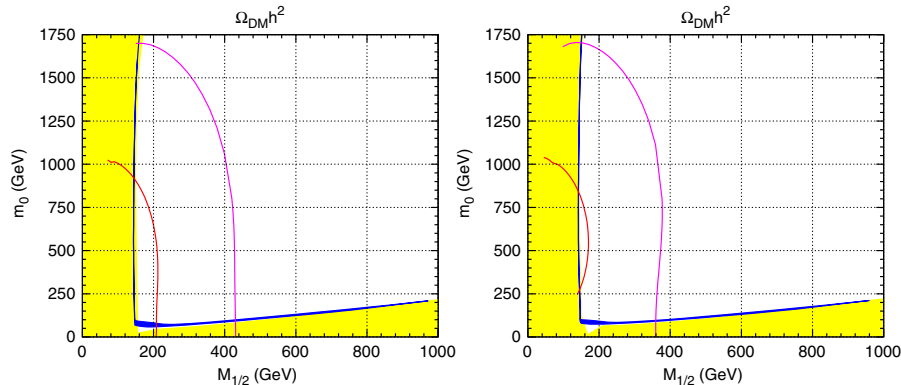
FIG. 4 (color online). Limits for mSUGRA with $\tan\beta = 10$, and $\mu > 0$ for $A_0 = -300$ GeV (left panel) and $A_0 = -500$ GeV (right panel). The blue regions are allowed by the DM constraint, for the explanation of the bounds see Fig. 2 and text.
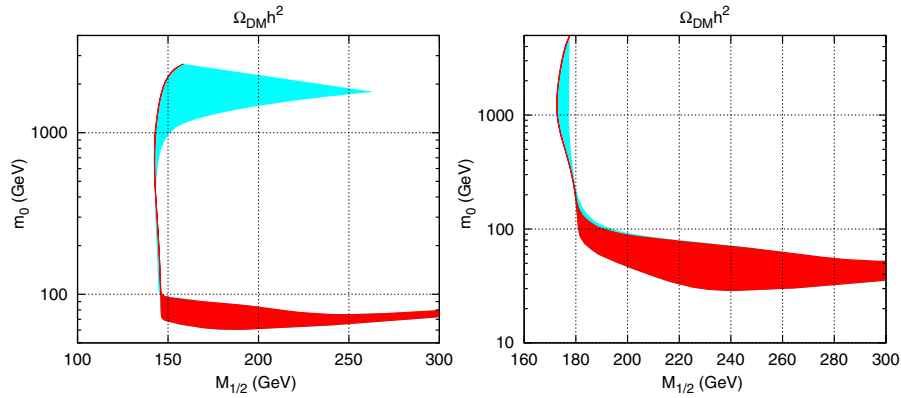
FIG. 5 (color online).   Logarithmically scaled zoom into the focus point region. In red the allowed region for $0.081 < \Omega h^2 < 0.129$ and in cyan the allowed region due the variation of $m_{\text{top}} = 171.2 \pm 2.1$ GeV. The left panel is for the mSUGRA case and the right panel for $M_T = 10^{15}$ GeV. The other parameters are taken at our standard values.

As mentioned above the uncertainty in the top mass is important for the calculation of the relic density. At low and moderate values of $\tan\beta$ the exact value of m_t affects mainly the focus point region. As Fig. 2 demonstrates near the focus point line the relic density changes very abruptly even for tiny changes of $M_{1/2}$. This is because a comparatively small value of μ is required to get a sufficiently enhanced coupling of the neutralino to the Z^0 boson. In mSUGRA the value of μ is determined from all other parameters by the condition of having correct EWSB and usually leads to $M_1, M_2 \ll \mu$. In the focus point region μ varies abruptly, points to the "left" of the focus point region are usually ruled out by the fact that EWSB cannot be achieved. Since m_t is the largest fermion mass, its exact value influences the value of μ required to achieve EWSB most. The change of μ with respect to a change of m_t then can lead to a significant shift in the DM allowed region of parameter space. This is demonstrated in Fig. 5, which shows a zoom into the focus point region for pure mSUGRA (to the left) and mSUGRA + **15** (to the right). The variation of the top mass shown corresponds to the current 1σ allowed range [3]. The pure mSUGRA is especially sensitive to a change of m_t. At large values of m_0 the uncertainty in "fixing" $M_{1/2}$ from the DM constraint can be larger than 100 GeV in the case of mSUGRA. Given this large uncertainty it would be impossible at present to distinguish the pure mSUGRA case from mSUGRA + seesaw, if the focus point region is the correct explanation of the observed DM. Note, however, that in the future the top mass will be measured more precisely. At the LHC one expects an uncertainty of 1–2 GeV [70] at a linear collider m_t could be determined down to an uncertainty of 100 MeV [71].

We now turn to a discussion of large $\tan\beta$. At large values of $\tan\beta$ the width of the CP-odd Higgs boson A becomes large, $\Gamma_A \sim M_A \tan^2\beta (m_b^2 + m_t^2)$, and a wide s-channel resonance occurs in the region $m_{\chi_1^0} \simeq M_A/2$. The enhanced annihilation cross section reduces $\Omega_{\chi_1^0} h^2$

to acceptable levels, the resulting region is known as the Higgs funnel region. In Fig. 6 we show the allowed range of parameters in the $(m_0, M_{1/2})$ plane for one specific value of $\tan\beta = 45$ and three different values of M_T. As demonstrated, the Higgs funnel region is very sensitive to the choice of M_T. It is fairly obvious that varying M_T one can cover nearly all of the plane, even for fixed values of all other parameters. We have calculated the DM allowed region for various values of $\tan\beta$ and found that the funnel appears for all $\tan\beta \gtrsim 40$, approximately.

The strong dependence of the Higgs funnel region on M_T unfortunately does not imply automatically that if large $\tan\beta$ is realized in nature one could get a very sensitive indirect "measurement" of the seesaw scale by determining $(m_0, M_{1/2})$. The reason is that the Higgs funnel is also very sensitive to the exact value of $\tan\beta$ and to the values (and errors) of the top and bottom quark mass. The latter is demonstrated in Fig. 7, where we show the DM allowed
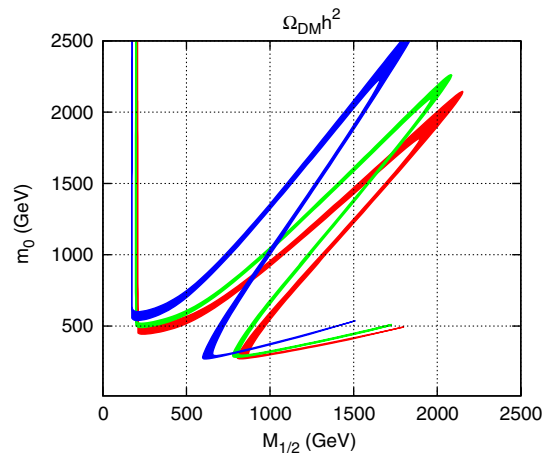

FIG. 6 (color online).   Allowed region for dark matter density in the $(m_0, M_{1/2})$ plane for $A_0 = 0$, $\mu \geq 0$ and $\tan\beta = 45$, for (from bottom to top) $M_T = 5 \times 10^{13}$ GeV (red), $M_T = 10^{14}$ (green) and $M_T = 10^{15}$ GeV (blue).
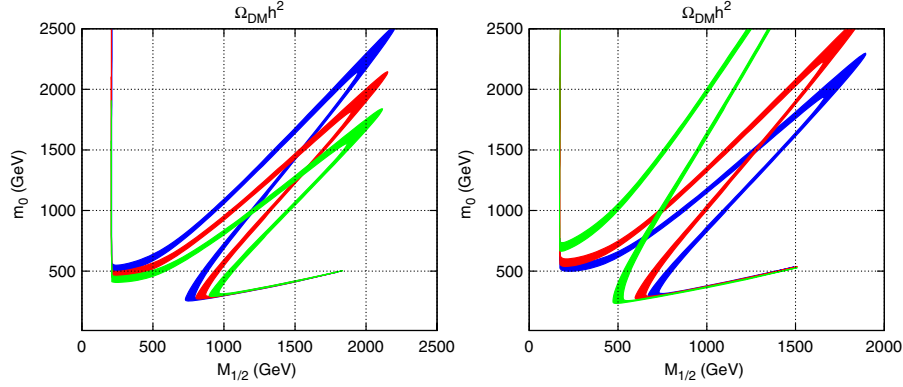
FIG. 7 (color online). Allowed region for the dark matter density in the $(m_0, M_{1/2})$ plane for $A_0 = 0$, $\mu \geq 0$ and $\tan\beta = 45$, for $M_T = 5 \times 10^{13}$ GeV and (to the left) for three values of $m_{\text{top}} = 169.1$ GeV (blue), $m_{\text{top}} = 171.2$ GeV (red) and $m_{\text{top}} = 173.3$ GeV (green). To the right: The same, but varying m_b. $m_{\text{bot}} = 4.13$ GeV (blue), $m_{\text{bot}} = 4.2$ GeV (red) and $m_{\text{bot}} = 4.37$ GeV (green).

range of parameters for a fixed choice of $\tan\beta$ and M_T varying to the left (to the right) m_t (m_b) within their current 1σ C.L. error band. The position of the funnel is especially sensitive to the exact value of m_b. Comparing Fig. 7 with Fig. 6 one can see that the uncertainty in m_b and m_t currently severely limits any sensitivity one could get on M_T. However, future determinations of m_b and m_t could improve the situation considerably. For future uncertainties in m_t see the discussion above for the focus point region. For m_b Ref. [72] estimates that m_b could be fixed to 4.17 ± 0.05 GeV, which might even be improved to an accuracy of $\Delta m_b \simeq 16$ MeV according to [73].

All of the above figures have been calculated using fixed values for λ_1 and λ_2 and negligibly small Yukawa couplings Y_T. This choice in general does not affect the calculation of the DM allowed regions much. However, a fully consistent calculation cannot vary M_T, Y_T and λ_2 independently, since this will lead to neutrino masses and angles outside the experimentally allowed ranges. Since Y_T is diagonalized by the same matrix as the effective neutrino mass matrix, m_ν, see the previous section, the measured

neutrino angles provide constraints on the relative size of the entries in Y_T. The absolute size of Y_T is then fixed for any fixed choice of λ_2 and M_T, once the neutrino spectrum is chosen to be hierarchical or quasidegenerate. In the numerical calculation shown in Fig. 8 we have chosen neutrino masses to be of the normal hierarchical type and fitted the neutrino angles to exact tribimaximal (TBM) values [15], i.e. $\tan^2\theta_{\text{Atm}} = 1$, $\tan^2\theta_\odot = 1/2$ and $\sin^2\theta_R = 0$. This has to be done in a simple iterative procedure, since the triplet parameters are defined at the high scale, whereas neutrino masses and angles are measured at low scale. For more details on the fit procedure see [35].

In Fig. 8 to the left we show two calculations of the DM allowed regions. The allowed range for negligibly small neutrino Yukawa couplings is shown by the filled (red) region, while the calculation with Y_T fitted to correctly explain solar and atmospheric neutrino data is the one inside the (blue) lines. Note the logarithmic scale. As demonstrated, the exact values of Y_T are of minor importance for the determination of the parameter region allowed by the DM constraint. Slightly larger differences
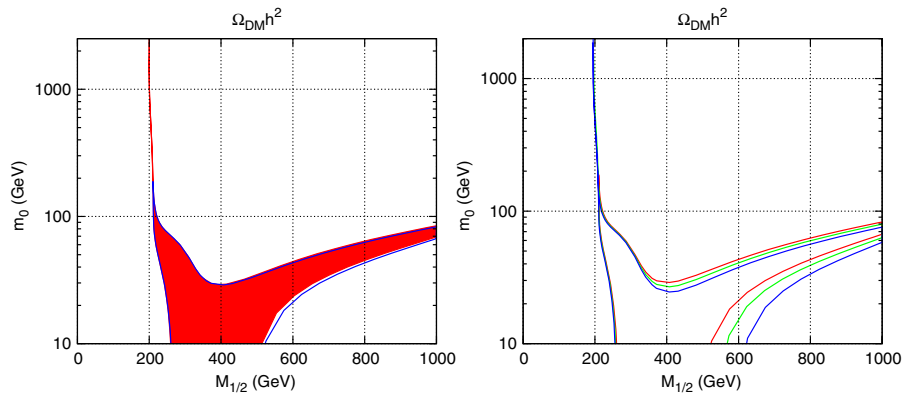

FIG. 8 (color online). Allowed region for dark matter density in the $(m_0, M_{1/2})$ plane for the "standard choice" of mSUGRA parameters for $M_T = 10^{14}$ GeV. To the left: For one fixed value of $\lambda_2 = 0.5$ the allowed range for negligibly small neutrino Yukawa couplings (red) and Y_T fitted to correctly explain solar and atmospheric neutrino data (blue lines). To the right: The DM allowed range of parameters for 3 different values of λ_2, $\lambda_2 = 0.5$ (red), $\lambda_2 = 0.75$ (green) and $\lambda_2 = 1$ (blue). Note the logarithmic scale.

between the fitted and unfitted calculations are found pushing M_T to larger values (see, however, below). For smaller values of M_T, the entries in Y_T needed to correctly explain neutrino data are smaller and, thus, Y_T affects the DM allowed region even less for $M_T < 10^{14}$ GeV.

In Fig. 8 to the right we compare three different calculations for λ_2, $\lambda_2 = 0.5$ (red), $\lambda_2 = 0.75$ (green) and $\lambda_2 = 1$ (blue), for fixed choice of other parameters. This plot serves to show that also the exact choice of λ_2 is of rather minor importance for the determination of the DM allowed region. Very similar results have been found for λ_1, we therefore do not repeat plots varying λ_1 here.

Finally, we will compare the constraints imposed on the parameter space of the model by $\Omega_{\mathrm{DM}} h^2$ with the constraints from the current data on nonobservation of lepton flavor violating processes. Since LFV within the present model has been studied in some detail in [35], we will not repeat all of the discussion here. Instead, here we concentrate on $\mu \to e\gamma$ exclusively, since the upper bound on $\mathrm{Br}(\mu \to e\gamma)$ of $\mathrm{Br}(\mu \to e\gamma) \leq 1.2 \times 10^{-11}$ [3] has been shown to provide currently the most important constraint.

In Fig. 9 we show the DM allowed parameter regions for $\tan\beta = 10$ and two values of M_T, $M_T = 5 \times 10^{13}$ GeV (to the left) and $M_T = 10^{14}$ GeV (to the right), for a fixed choice of all other parameters. Superimposed on this plot are lines of constant branching ratio for $\mathrm{Br}(\mu \to e\gamma)$. The latter have been calculated requiring neutrino masses being hierarchical and fitted to solar and atmospheric neutrino mass squared differences and neutrino angles fitted to TBM values. Within the $(m_0, M_{1/2})$ region shown, $\mathrm{Br}(\mu \to e\gamma)$ can vary by 2 orders of magnitude, depending on the exact combination of $(m_0, M_{1/2})$, even for all other parameters fixed. The most important parameter determining $\mathrm{Br}(\mu \to e\gamma)$, once neutrino data is fixed, however, is M_T, as can be seen comparing the figure to the left with the plot on the right. While for $M_T = 10^{14}$ GeV about ''half'' of the plane is ruled out by the nonobservation of $\mu \to e\gamma$, for

$M_T = 5 \times 10^{13}$ GeV with the current upper limit nearly all of the plane becomes allowed. The strong dependence of $\mu \to e\gamma$ on M_T can be understood from the analytical formulas presented in [35]. In this paper it was shown that $\mathrm{Br}(\mu \to e\gamma)$ scales very roughly as $\mathrm{Br}(\mu \to e\gamma) \propto M_T^4 \log(M_T)$, if neutrino masses are to be explained correctly. For $\tan\beta = 10$ one thus concludes that with present data values of M_T larger than (few) 10^{13} GeV– (few) 10^{14} GeV are excluded by $\mathrm{Br}(\mu \to e\gamma)$, to be compared with $M_T/\lambda_2 \lesssim 10^{15}$ GeV from the measured neutrino masses. Note, however, that (i) the constraint from neutrino masses is relatively independent of $\tan\beta$, m_0 and $M_{1/2}$, while $\mu \to e\gamma$ shows strong dependence on these parameters; and (ii) allowing the value of the reactor angle $\sin^2\theta_R$ to vary up to its experimental upper limit, $\sin^2\theta_R = 0.056$ [14], leads to larger values of $\mathrm{Br}(\mu \to e\gamma)$ and thus to a tighter upper limit on M_T.

In Fig. 10 we show the results for a calculation comparing dark matter and LFV in the case of large $\tan\beta$. Here the same constraints as in Fig. 9 are shown, however for $\tan\beta = 45$. Again we show the calculation for two values of M_T, since M_T is the most important free parameter. It is known that at large values of $\tan\beta$, LFV decays are enhanced due to an enhanced chargino diagram, which in the limit of large $\tan\beta$ scales approximately as $\tan^2\beta$ [28]. Therefore, constraints on the parameter space from nonobservation of LFV decays are more severe in the case of large $\tan\beta$, leading to tighter upper limits on M_T. This is clear if we compare Figs. 9 and 10, noticing the different scales. However, because of the Higgs funnel region developing for large $\tan\beta$, the interesting part of the parameter space enlarges compensating for the larger values of the LFV decays. This can be seen in Fig. 10, where for $M_T = 5 \times 10^{13}$ GeV (left), most of the $(m_0, M_{1/2})$ plane is allowed by the upper limit on $\mathrm{Br}(\mu \to e\gamma)$, while for $M_T = 10^{14}$ GeV (right), about half of the plane is ruled out by this limit.
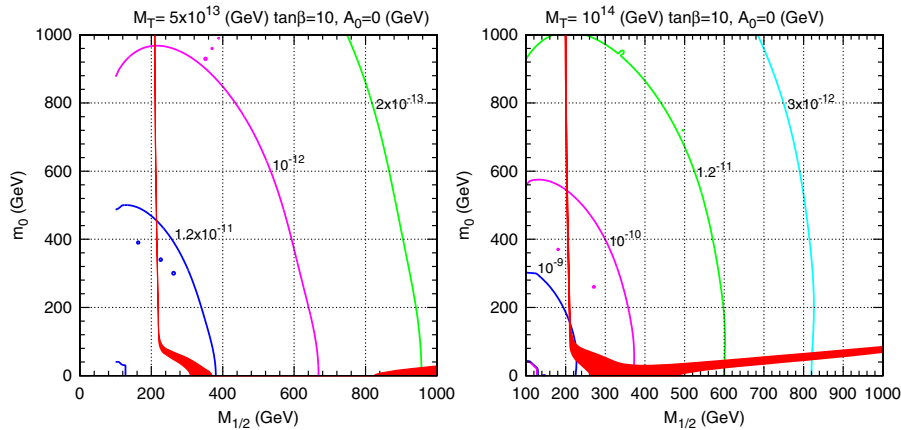

FIG. 9 (color online). Allowed region for dark matter density in the $(m_0, M_{1/2})$ plane for our ''standard choice'' of mSUGRA parameters and for two values of M_T: $M_T = 5 \times 10^{13}$ (left panel) and for $M_T = 10^{14}$ (right panel). Superimposed are the contour lines for the $\mathrm{Br}(\mu \to e\gamma)$.
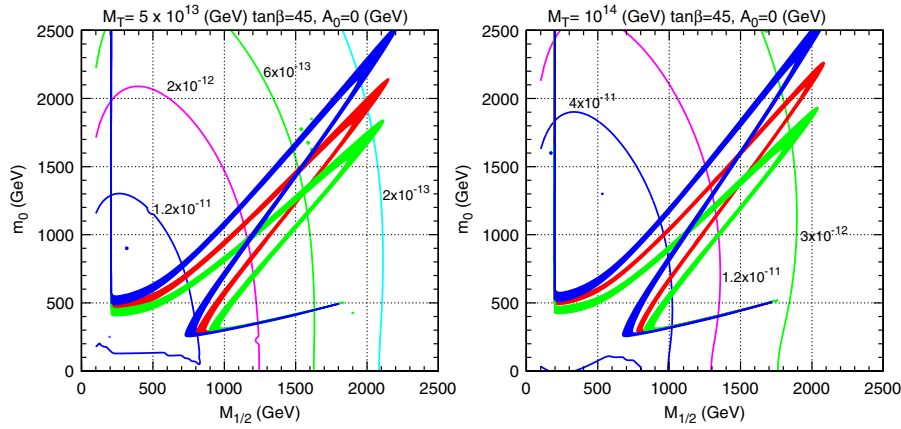
FIG. 10 (color online).   Allowed region for dark matter density ($0.081 < \Omega_{\chi_1^0} h^2 < 0.129$) in the ($m_0, M_{1/2}$) plane for $A_0 = 0$, $\mu \geq 0$ and $\tan\beta = 45$, for three values of $m_{\text{top}} = 169.1$ GeV (blue), $m_{\text{top}} = 171.2$ GeV (red) and $m_{\text{top}} = 173.3$ GeV (green) for $M_T = 5 \times 10^{13}$ (left panel) and for $M_T = 10^{14}$ (right panel). Superimposed are the contour lines for the $\text{Br}(\mu \to e\gamma)$.

We have concentrated in this paper on discussing DM in mSUGRA with a seesaw type-II. Before closing this section, we would like to briefly comment on the case of seesaw type-I. In seesaw type-I one adds two or more singlet superfields to the superpotential of the MSSM. These singlets have Yukawa couplings to the standard model lepton doublet and a Majorana mass term, but no other couplings to any of the MSSM fields. The running of the mSUGRA soft parameters in this setup is therefore only changed by the neutrino Yukawa couplings. Just as in the seesaw type-II one can estimate from current neutrino data that the Yukawa couplings are order $Y^\nu \sim \mathcal{O}(1)$ for the right-handed Majorana mass order $\mathcal{O}(10^{15})$ GeV.[4] For any M_M smaller than this number, one therefore expects that the running of the soft parameters is essentially mSUGRA-like. (Apart from small off-diagonal terms in m_L^2, which are exactly zero in mSUGRA.) This implies that also the DM regions should be very close to those found in the mSUGRA case. We have confirmed this expectation by calculating the DM allowed region for our standard choice of mSUGRA parameters and various values of the right-handed neutrino masses. Even for Y^ν at the upper limit allowed by perturbativity we did not find any significant departure from the mSUGRA case. With the hindsight of the results shown in Fig. 8 for the seesaw type-II this is not surprising.

One exceptional case for the seesaw type-I has been discussed, however, recently in [58]. The authors of [58] observed that for Yukawa couplings close to 1 and a large value of the common trilinear A_0, say $A_0 = 1100$ GeV, the left sneutrinos can be the next-to-LSP (NLSP) for small-to-moderate values of m_0, $M_{1/2}$ and $\tan\beta$. For a sneutrino NLSP nearly degenerate with the lightest neutralino a new

coannihilation regions then shows up at small values of m_0. We have repeated this calculation with three right-handed neutrinos ([58] use only one singlet superfield) and confirm the sneutrino coannihilation region for $|Y^\nu| \simeq \mathcal{O}(1)$ and large A_0. However, in our calculation, if we insist on fitting the large atmospheric and solar angles, all of the region is excluded by upper limits on LFV decays, if we put the matrix R of the Casas-Ibarra parametrization for the neutrino Yukawa couplings [74] to the identity matrix. As has been shown in [29,31], we could, in principle, avoid these strong constraints from LFV by a careful adjustments of the unknown parameters in R. We did, however, not attempt to do a systematic study as to how R has to be chosen that the sneutrino coannihilation becomes consistent with LFV decays.

IV. CONCLUSIONS

In conclusion, we have calculated the neutralino relic density in a supersymmetric model with mSUGRA boundary conditions including a type-II seesaw mechanism to explain current neutrino data. We have discussed how the allowed ranges in mSUGRA parameter space change as a function of the seesaw scale. The stau coannihilation region is shifted towards smaller m_0 for smaller values of the triplet mass M_T, while the bulk region and the focus point line are shifted towards larger values of $M_{1/2}$ for M_T sufficiently below the GUT scale. The Higgs funnel, which appears at large values of $\tan\beta$ has turned out to be especially sensitive to the value of M_T. Determining $M_{1/2}$ from the mass of any gaugino and m_0 from a sparticle which is *not important for the DM calculation*, one could, therefore, get a constraint on M_T from the requirement that the observed $\Omega_{\text{DM}} h^2$ is correctly explained by the calculated $\Omega_{\chi_1^0} h^2$.

On the positive side, we can remark that current data on neutrino masses put an upper bound on M_T of the order of $\mathcal{O}(10^{15})$ GeV. Since this is at least 1 order of magnitude

---

[4]Different from the seesaw type-II, where Y_T depends linearly on M_T, however, in seesaw type-I Yukawas scale like $Y^\nu \sim \sqrt{M_M}$.

smaller than the GUT scale, the characteristic shifts in the DM regions are necessarily nonzero if our setup is the correct explanation of the observed neutrino oscillation data. Even more stringent upper limits on M_T follow, in principle, from the nonobservation of LFV decays. A smaller M_T implies larger shifts of the DM region. However, the "exact" upper limit on M_T from LFV decays depends strongly on $\tan\beta$, m_0 and $M_{1/2}$, and thus can be quantified only when at least some information on these parameters is available.

On the downside, we need to add a word of caution. We have found that the DM calculation suffers from a number of uncertainties, even if we assume the soft masses to be perfectly known. The most important SM parameters turn out to be the bottom and the top quark mass. The focus point line depends extremely sensitively on the exact value of the top mass, the Higgs funnel shows a strong sensitivity on both m_b and m_t.

Finally, it is clear that quite accurate sparticle mass measurements will be necessary, before any quantitative conclusions can be taken from the effects we have discussed. Unfortunately, such accurate mass measurements might be very difficult to come by for different reasons. In the focus point region all scalars will be heavy, leading to small production cross section at the LHC. In the coanni-

hilation line with a nearly degenerate stau and a neutralino, the stau decays produce very soft taus, which are hard for the LHC to measure. And the Higgs funnel extends, depending on $\tan\beta$ and M_T, to very large values of $(m_0, M_{1/2})$, at least partially outside the LHC reach. Nevertheless, DM provides in principle an interesting constraint on the (supersymmetric) seesaw explanation of neutrino masses, if seesaw type-II is realized in nature, a fact which to our knowledge has not been discussed before in the literature.

ACKNOWLEDGMENTS

[1] G. Jungman, M. Kamionkowski, and K. Griest, Phys. Rep. **267**, 195 (1996).
[2] G. Bertone, D. Hooper, and J. Silk, Phys. Rep. **405**, 279 (2005).
[3] C. Amsler *et al.*, Phys. Lett. B **667**, 1 (2008); http:// pdg.lbl.gov/.
[4] D. N. Spergel *et al.* (WMAP Collaboration), Astrophys. J. Suppl. Ser. **148**, 175 (2003).
[5] E. Komatsu *et al.* (WMAP Collaboration), Astrophys. J. Suppl. Ser. **180**, 330 (2009).
[6] M. Tegmark *et al.* (SDSS Collaboration), Phys. Rev. D **74**, 123507 (2006).
[7] L. Bergstrom, arXiv:0903.4849.
[8] H. Baer, E. K. Park, and X. Tata, arXiv:0903.0555.
[9] Y. Fukuda *et al.* (Super-Kamiokande Collaboration), Phys. Rev. Lett. **81**, 1562 (1998).
[10] Q. R. Ahmad *et al.* (SNO Collaboration), Phys. Rev. Lett. **89**, 011301 (2002).
[11] K. Eguchi *et al.* (KamLAND Collaboration), Phys. Rev. Lett. **90**, 021802 (2003).
[12] MINOS Collaboration, arXiv:0708.1495.
[13] KamLAND Collaboration, Phys. Rev. Lett. **100**, 221803 (2008).
[14] For a review of neutrino oscillation data, see M. Maltoni, T. Schwetz, M. A. Tortola, and J. W. F. Valle, New J. Phys. **6**, 122 (2004); an updated analysis has now been published in T. Schwetz, M. Tortola, and J. W. F. Valle, New J. Phys.

10, 113011 (2008) where all experimental references can be found.
[15] P. F. Harrison, D. H. Perkins, and W. G. Scott, Phys. Lett. B **530**, 167 (2002).
[16] S. Weinberg, Phys. Rev. Lett. **43**, 1566 (1979); Phys. Rev. D **22**, 1694 (1980).
[17] E. Ma, Phys. Rev. Lett. **81**, 1171 (1998).
[18] P. Minkowski, Phys. Lett. B **67**, 421 (1977).
[19] T. Yanagida, in *KEK Lectures*, edited by O. Sawada and A. Sugamoto (KEK, Tsukuba, 1979); M. Gell-Mann, P. Ramond, and R. Slansky, in *Supergravity*, edited by P. van Niewenhuizen and D. Freedman (North-Holland, Amsterdam, 1979).
[20] R. N. Mohapatra and G. Senjanovic, Phys. Rev. Lett. **44**, 912 (1980).
[21] J. Schechter and J. W. F. Valle, Phys. Rev. D **22**, 2227 (1980).
[22] T. P. Cheng and L. F. Li, Phys. Rev. D **22**, 2860 (1980).
[23] G. Lazarides, Q. Shafi, and C. Wetterich, Nucl. Phys. **B181**, 287 (1981).
[24] R. N. Mohapatra and G. Senjanovic, Phys. Rev. D **23**, 165 (1981).
[25] R. Foot, H. Lew, X. G. He, and G. C. Joshi, Z. Phys. C **44**, 441 (1989).
[26] F. Borzumati and A. Masiero, Phys. Rev. Lett. **57**, 961 (1986).

[27] J. Hisano, T. Moroi, K. Tobe, M. Yamaguchi, and T. Yanagida, Phys. Lett. B **357**, 579 (1995).

[28] J. Hisano, T. Moroi, K. Tobe, and M. Yamaguchi, Phys. Rev. D **53**, 2442 (1996).

[29] J. R. Ellis, J. Hisano, M. Raidal, and Y. Shimizu, Phys. Rev. D **66**, 115013 (2002).

[30] F. Deppisch, H. Pas, A. Redelbach, R. Ruckl, and Y. Shimizu, Eur. Phys. J. C **28**, 365 (2003).

[31] E. Arganda and M. J. Herrero, Phys. Rev. D **73**, 055003 (2006).

[32] S. Antusch, E. Arganda, M. J. Herrero, and A. M. Teixeira, J. High Energy Phys. 11 (2006) 090.

[33] E. Arganda, M. J. Herrero, and A. M. Teixeira, J. High Energy Phys. 10 (2007) 104.

[34] A. Rossi, Phys. Rev. D **66**, 075003 (2002).

[35] M. Hirsch, S. Kaneko, and W. Porod, Phys. Rev. D **78**, 093004 (2008).

[36] J. Hisano, M. M. Nojiri, Y. Shimizu, and M. Tanaka, Phys. Rev. D **60**, 055008 (1999).

[37] N. V. Krasnikov, Phys. Lett. B **388**, 783 (1996).

[38] N. Arkani-Hamed, H. C. Cheng, J. L. Feng, and L. J. Hall, Phys. Rev. Lett. **77**, 1937 (1996).

[39] D. Nomura, Phys. Rev. D **64**, 075001 (2001).

[40] W. Porod and W. Majerotto, Phys. Rev. D **66**, 015003 (2002).

[41] F. Deppisch, H. Pas, A. Redelbach, R. Ruckl, and Y. Shimizu, Phys. Rev. D **69**, 054014 (2004).

[42] F. del Aguila *et al.*, Eur. Phys. J. C **57**, 183 (2008).

[43] F. Deppisch, H. Pas, A. Redelbach, and R. Ruckl, Phys. Rev. D **73**, 033004 (2006).

[44] A. Bartl, K. Hidaka, K. Hohenwarter-Sodek, T. Kernreiter, W. Majerotto, and W. Porod, Eur. Phys. J. C **46**, 783 (2006).

[45] M. Hirsch, J. W. F. Valle, W. Porod, J. C. Romao, and A. Villanova del Moral, Phys. Rev. D **78**, 013006 (2008).

[46] E. Carquin, J. Ellis, M. E. Gomez, S. Lola, and J. Rodriguez-Quintero, J. High Energy Phys. 05 (2009) 026.

[47] J. N. Esteves, J. C. Romao, A. Villanova del Moral, M. Hirsch, J. W. F. Valle, and W. Porod, J. High Energy Phys. 05 (2009) 003.

[48] G. A. Blair, W. Porod, and P. M. Zerwas, Eur. Phys. J. C **27**, 263 (2003).

[49] A. Freitas, W. Porod, and P. M. Zerwas, Phys. Rev. D **72**, 115002 (2005).

[50] M. R. Buckley and H. Murayama, Phys. Rev. Lett. **97**, 231801 (2006).

[51] J. R. Ellis, J. S. Hagelin, D. V. Nanopoulos, K. A. Olive, and M. Srednicki, Nucl. Phys. **B238**, 453 (1984).

[52] K. Griest and D. Seckel, Phys. Rev. D **43**, 3191 (1991).

[53] M. Drees and M. M. Nojiri, Phys. Rev. D **47**, 376 (1993).

[54] G. B. Gelmini and P. Gondolo, Phys. Rev. D **74**, 023510 (2006).

[55] B. C. Allanach, G. Belanger, F. Boudjema, and A. Pukhov, J. High Energy Phys. 12 (2004) 020.

[56] H. Baer, C. Balazs, and A. Belyaev, J. High Energy Phys. 03 (2002) 042.

[57] J. L. Feng, K. T. Matchev, and T. Moroi, Phys. Rev. D **61**, 075005 (2000).

[58] K. Kadota, K. A. Olive, and L. Velasco-Sevilla, Phys. Rev. D **79**, 055018 (2009).

[59] F. Joaquim and A. Rossi, Phys. Rev. Lett. **97**, 181801 (2006).

[60] For reviews on mSUGRA and MSSM, see for example, H. P. Nilles, Phys. Rep. **110**, 1 (1984); H. E. Haber and G. L. Kane, Phys. Rep. **117**, 75 (1985); S. P. Martin, arXiv:hep-ph/9709356.

[61] S. P. Martin and M. T. Vaughn, Phys. Rev. D **50**, 2282 (1994); **78**, 039903 (2008).

[62] W. Porod, Comput. Phys. Commun. **153**, 275 (2003).

[63] G. Belanger, F. Boudjema, A. Pukhov, and A. Semenov, Comput. Phys. Commun. **176**, 367 (2007).

[64] G. Belanger, F. Boudjema, A. Pukhov, and A. Semenov, Comput. Phys. Commun. **174**, 577 (2006).

[65] The latest version of SPHENO can be obtained from http://theorie.physik.uni-wuerzburg.de/porod/SPheno.html

[66] http://wwwlapp.in2p3.fr/lapth/micromegas/

[67] B. C. Allanach, A. Djouadi, J. L. Kneur, W. Porod, and P. Slavich, J. High Energy Phys. 09 (2004) 044.

[68] S. Heinemeyer, W. Hollik, H. Rzehak, and G. Weiglein, Eur. Phys. J. C **39**, 465 (2005).

[69] M. Frank, T. Hahn, S. Heinemeyer, W. Hollik, H. Rzehak, and G. Weiglein, J. High Energy Phys. 02 (2007) 047. The FEYNHIGGS code can be found at: http://www.feynhiggs.de/

[70] G. Aad *et al.* (ATLAS Collaboration), arXiv:0901.0512.

[71] J. A. Aguilar-Saavedra *et al.* (ECFA/DESY LC Physics Working Group), arXiv:hep-ph/0106315.

[72] N. Brambilla *et al.* (Quarkonium Working Group), arXiv:hep-ph/0412158.

[73] K. G. Chetyrkin, J. H. Kuhn, A. Maier, P. Maierhofer, P. Marquard, M. Steinhauser, and C. Sturm, Phys. Rev. D **80**, 074010 (2009).

[74] J. A. Casas and A. Ibarra, Nucl. Phys. **B618**, 171 (2001).